Biosensors and Bioelectronics 130 (2019) 262–268

Contents lists available at ScienceDirect

Biosensors and Bioelectronics

journal homepage: www.elsevier.com/locate/bios

An ultrasensitive aptasensor based on self-enhanced Au nanoclusters as highly efficient electrochemiluminescence indicator and multi-site landing DNA walker as signal amplification

Fang Yang[a,1], Xia Zhong[a,1], Xinya Jiang[a,b], Ying Zhuo[a], Ruo Yuan[a,*], Shaping Wei[a,*]

[a] Key Laboratory of Luminescent and Real-Time Analytical Chemistry (Southwest University), Ministry of Education, College of Chemistry and Chemical Engineering, Southwest University, Chongqing 400715, PR China

[b] Chongqing Key Laboratory of Inorganic Special Functional Materials, College of Chemistry and Chemical Engineering, Yangtze Normal University, Chongqing 408100, PR China

ARTICLE INFO

Keywords:
Electrochemiluminescence
Self-enhanced Au nanoclusters
N,N-diisopropylethylenediamine
Multi-site landing DNA walker

ABSTRACT

Gold nanoclusters (Au NCs) have been shown to be prospective nanoscale electrochemiluminescence (ECL) materials that are being extensively explored in bioanalysis. However, the low ECL efficiency of Au NCs has been a bottleneck barrier for their better bioapplications. To overcome this disadvantage, a low oxidation potential co-reactant *N,N*-diisopropylethylenediamine (DPEA) was first used to prepare self-enhanced Au NCs (Au-DPEA NCs) for drastically enhancing the ECL efficiency of Au NCs in this study. In addition, an efficient multi-site landing DNA walker with multidirectional motion track and rapid payloads release compared to directional DNA walker was constructed for converting target mucin 1 (MUC1) to intermediate DNA and achieving significant signal amplification. On the basis of the Au-DPEA NCs as efficient ECL signal labels and multi-site landing DNA walker as signal amplification strategy, an ECL aptasensor was established for the ultrasensitive detection of MUC1 in the range from 1 fg mL^{-1} to 1 ng mL^{-1} with a limit of detection down to 0.54 fg mL^{-1}. The results demonstrated that the present study opened a new research direction for the development of high-efficiency Au NCs indicator as well as ultrasensitive ECL sensing platform for applications in clinical and bioanalysis.

1. Introduction

Metal nanoclusters (NCs) with size comparable to the Fermi wavelength of the electron exhibit molecular-like properties of discrete electronic states (Schmid et al., 1999). Among them, gold nanoclusters (Au NCs), in particular, have attracted considerable research interest in various areas (such as cell labeling, biological imaging and biosensing) due to their facile synthetic procedure, good chemical stability, low toxicity, and excellent biocompatibility (Lin et al., 2010; Li and Ulrich Nienhaus, 2012; Chen et al., 2013; Song et al., 2015). Recently, extensive research works have been carried out on the practical applications of Au NCs through the electrochemiluminescence (ECL) sensing technique. For example, Zhu's group developed an Au NCs-based ECL sensor to detect dopamine in the presence of co-reactant $S_2O_8^{2-}$ (Li et al., 2011). Chen's group achieved the sensitive detection of Pb^{2+} based on the ECL of Au NCs using triethyamine (TEA) as co-reactant (Fang et al., 2011). The ECL intensities of Au NCs in these works were significantly improved by additional co-reactants, but the ECL signals obtained from the intermolecular interaction suffered from poor stability, high loss of energy and low efficiency (H.J. Wang et al., 2015; L. Wang et al.,2015). Therefore, to develop Au NCs with high efficiency is a critical factor in expanding its bioanalytical applications. Self-enhanced ECL pattern, in which the co-reactant species and luminophore present in one molecular via covalent linking, has been demonstrated to exhibit high ECL efficiency and is very popular in the bioanalytical field. (Liang et al., 2015; Chen et al., 2015; Fu et al., 2017). This ECL pattern is highly advantageous in enhancing ECL signal compared to the intermolecular reaction pattern because it shortens the electronic transmission distance, eliminates the use of excess co-reactants and reduces the loss of energy (Li et al., 2015; Swanick et al., 2012). Recently, Wang and colleague[s] used *N,N*-Diethylethylenediamine (DEDA) as co-reactant to synthesize self-enhanced Au NCs (Au-DEDA NCs) for enhancing the ECL intensity of Au NCs (Wang et al., 2016). However, the high oxidation potential of DEDA restricted the further improvement in ECL performance of Au NCs. Therefore, a low oxidation potential co-reactant *N,N*-diisopropylethylenediamine (DPEA) was first

* Corresponding authors.
E-mail addresses: yuanruo@swu.edu.cn (R. Yuan), shapingw@swu.edu.cn (S. Wei).
[1] These authors contributed equally.

https://doi.org/10.1016/j.bios.2019.01.057
Received 14 September 2018; Received in revised form 3 January 2019; Accepted 21 January 2019
Available online 01 February 2019
0956-5663/

employed to synthesize high efficiency self-enhanced Au NCs (Au-DPEA NCs) which were further used to construct an ultrasensitive ECL platform for MUC1 detection.

DNA with diversity and exquisite specificity has been widely used to design various DNA-based machines such as “DNA nippers” (Yue et al., 2017; Zhang et al., 2018) “DNA walkers” (Jung et al., 2016; H.J. Wang et al., 2015; L. Wang et al., 2015; Zhou et al., 2015) and “DNA motors” (Cha et al., 2014; Wickham et al., 2012). Recently, DNA-based walker machines have captured considerable attractions for their outstanding locomotion and controllability. For instance, Turberfield et al. constructed a restriction endonuclease powered DNA walker that moved on a specific DNA track (Bath et al., 2005b). Salaita et al. designed a directional DNA walker using RNase H as energy source, which moved along a RNA track (Yehl et al., 2016). Despite these DNA walkers have been demonstrated to present several advantages over traditional DNA amplification such as the structural simplicity and easy construction, they also accompanied with several drawbacks: (i) the motion of the walker was directional, which restrained the release of payloads in a certain degree, (ii) the driving force of the walker was endonucleases, which had low hydrolysis rate toward the substrate. To overcome these disadvantages, we constructed an Exo III propelled multi-site landing DNA walker, in which the walker could move along the multi-directional track by the high hydrolysis rate of Exo III toward substrate (Bath et al., 2005a) and then achieved rapid payloads release. In this way, the multi-site landing DNA walker could be acted as an excellent signal amplification tool for biodetection.

In this work, we prepared a self-enhanced Au-DPEA NCs-based ECL aptasensor for sensitive detection of target MUC1 with aid of an effective Exo III propelled multi-site landing DNA walker for signal amplification. As shown in Scheme 1, briefly, the thioctic acid (TA)-capped Au NCs (Au-TA NCs) were synthesized by one-step reduction of gold precursor using sodium borohydride ($NaBH_4$) in aqueous solution, followed by covalent linking with co-reactant DPEA to form the high efficiency self-enhanced Au NCs (Au-DPEA NCs). Subsequently, through the Ag-S covalent bond, Fc-labeled quench probe (Fc-HP) was immobilized onto Ag and Au-DPEA NCs modified glassy carbon electrode (GCE) to gain signal “switch off” state. Then, plenty of mimic targets obtained from walker process hybridized with Fc-HP to initiate another Exo III cleavage process, accompanied with signal “switch on” state as Fc left from the modified electrode. The aptasensor integrated the advantages of self-enhanced Au-DPEA NCs and the multi-site landing DNA walker machine to achieve satisfactory ECL performance and broadened the application of metal NCs in ultrasensitive biodetection.

2. Experimental section

2.1. Materials and reagents

Hexanethiol (HT) and poly-(diallyldimethylammonium chloride) (PDDA) were purchased from Sigma-Aldrich Co. (St. Louis, MO, USA). Sodium borohydride ($NaBH_4$), polyvinylpyrrolidoneK30 (PVPK30), chitosan (CS), sodium citrate ($Na_3C_6H_5O_7{\cdot}2H_2O$), Iron (III) chloride hexahydrateand ($FeCl_3{\cdot}6H_2O$), polyethylene glycol-800 (PEG-800), acetic acid (NaAc), and polyethylene glycol-400 (PEG-400) were acquired from Chengdu Kelong Chemical Industry (Chengdu, China). Silver nitrate ($AgNO_3$) and sodium hydroxide (NaOH) were purchased from Sinopharm Chemical Reagent Company (Shanghai, China). *N,N*-diisopropylethylenediamine (DPEA, 97%), thioctic acid (TA, 98%), and

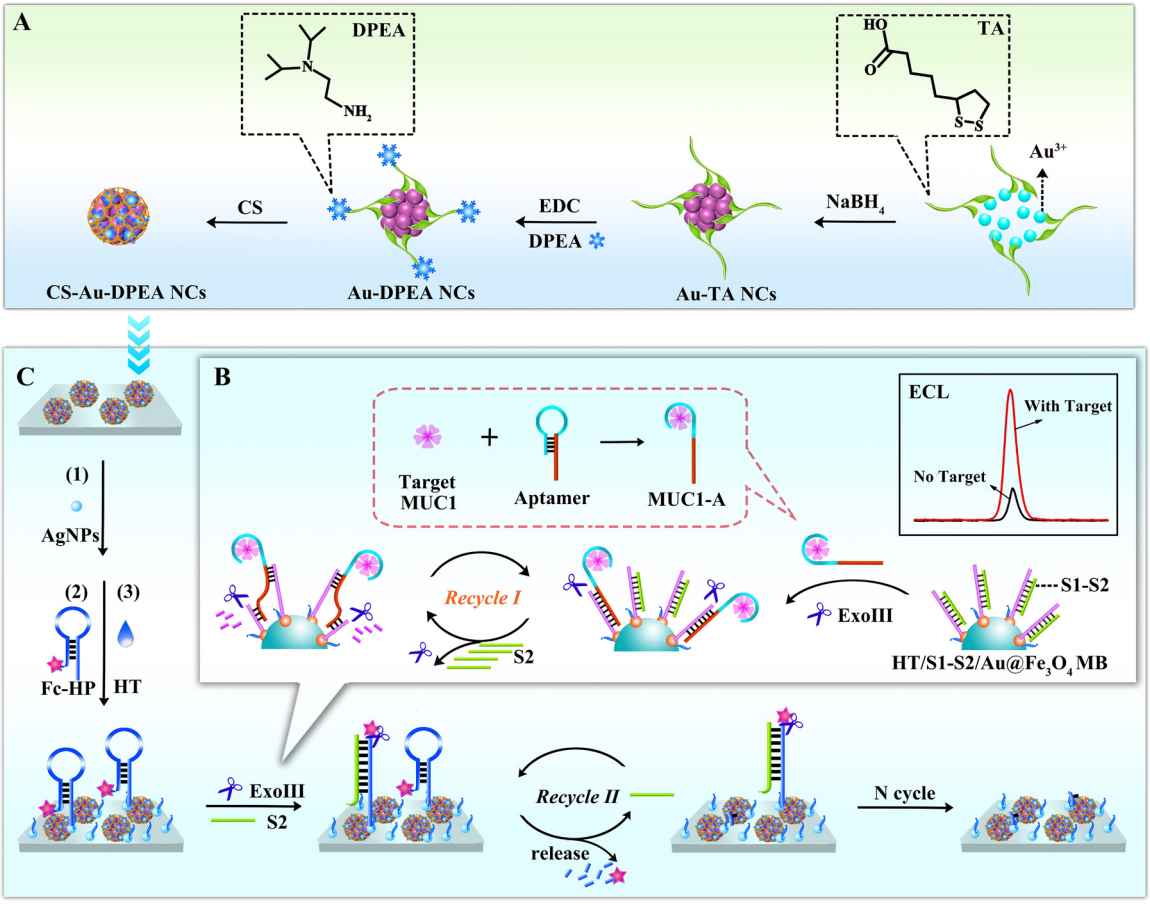

Scheme 1. Schematic illustration of (A) preparation of chitosan-encapsulated self-enhanced Au-DPEA NCs, (B) amplification strategy for target MUC1 conversion, (C) fabrication of the aptasensor.

N,N-Diethylethylenediamine (DEDA, 99%) were bought from J&K Technology Co., Ltd. (Beijing, China). 1-(3-(Dimethylamino)propyl)-3-ethylcarbodiimide hydrochloride (EDC) was supplied by Shanghai Medpep Co. (Shanghai, China). Gold chloride tetrahydrate ($HAuCl_4{\cdot}4H_2O$, 99.9%) was supplied by Chongqing Chemical Reagent Co. (Chongqing, China). Human mucin1 (MUC1) was supplied by North Connaught Biotechnology Co., Ltd. (Shanghai, China). The buffers involved in this work were as follows: The 0.1 M phosphate buffered saline (PBS, pH 8.0) was prepared with 0.08 M Na_2HPO_4, 0.02 M KH_2PO_4 and 0.1 M KCl; 20 mM Tris-HCl was prepared with 140 mM NaCl, 5 mM KCl, 1 mM $CaCl_2$, and 1 mM $MgCl_2$, (pH 7.4). Exo III and all the oligonucleotides with different sequences were synthesized by Sangon Biological Engineering Technology and Services Co.,Ltd. (Shanghai, China), and the oligonucleotides sequences were summarized in the Supplementray Material.

2.2. Apparatus

The ECL responses were recorded in PBS buffer with a MPI-A ECL analyzer (Xi' an Remax Electronics, China). The modified glassy carbon electrode (GCE, $\Phi = 4$ mm) was acted as working electrode in the three-electrode system in which the Ag/AgCl (sat. KCl) as reference electrode and platinum wire as counter electrode. Cyclic voltammetry (CV) was performed on a CHI 660C electrochemistry workstation (CHI Instruments of Shanghai, China). The morphology characterization of synthesized materials was completed with a scanning electron microscopy (SEM, S-4800, Hitachi, Japan) and high-resolution transmission electron microscopy (HRTEM, FEI Tecnai G2 F20, U.S.A.), respectively. An UV−vis spectrophotometer (S UV-2450, himadzu, Tokyo, Japan) and an F-5700 spectrofluorophotometer (Hitachi, Tokyo, Japan) were used to characterize the optical properties of Au NCs and Au-DPEA NCs, respectively.

2.3. Synthesis of self-enhanced Au nanoclusters (Au-DPEA NCs)

First, the Au nanoclusters stabilized by thioctic acid (Au-TA NCs) were synthesized according to the method introduced by Mattoussi with some modification (Aldeek et al., 2013). Briefly, TA (0.15 mM) was dissolved in 20 mL of ultrapure water containing 100 μL of 1 M NaOH, followed by adding 1% $HAuCl_4$ solution (n_{Au}:n_{TA} = 1:3) under vigorous stirring. After stirring for 4 h, 400 μL of 50 mM $NaBH_4$ was added dropwise. The mixture was stirred for another 4 h and disposed with membrane tubing of 3.5 K molecular weight cutoff (MWCO) for 48 h (refresh ultrapure water every 8 h).

Then, self-enhanced Au-DPEA NCs were synthesized according to the method with some modification (Wang et al., 2016). First, 0.0383 g of EDC was added into the 5 mL of Au-TA NCs dispersion with stirring for 2 h at room temperature. Subsequently, 35 μL of DPEA was introduced, and the reaction was allowed to proceed overnight. Last, the as-synthesized Au-DPEA NCs were treated with membrane tubing (3.5 K MWCO) for 48 h and dispersed in 2 mL of 0.5% CS after the removal of solvent in vacuum oven.

2.4. Preparation of the multi-site landing DNA walker

First, the S1-S2 duplex was generated by annealing the solution of S1 (5 μM) and S2 (5 μM) at 95 °C for 5 min, followed by cooling down to 37 °C over 3 h. (Yang et al., 2017). Then, the S1-S2 duplex was added into the Au@Fe_3O_4 magnetic nanoparticles solution (120 μL) to form the S1-S2/Au@Fe_3O_4 bioconjugates via Au-S bond under gentle shaking at 4 °C for 16 h, followed by adding 1 mM HT to block nonspecific binding sites of AuNPs. After removing excess S1-S2 duplex and HT by magnetic separation, the S1-S2/Au@Fe_3O_4 bioconjugates were redispersed in 200 μL of Tris-HCl buffer and stored at 4 °C for further use. 10 μL of S1-S2/Au@Fe_3O_4 bioconjugates solution reacted with 10 μL mixture containing aptamer and various concentrations of MUC1 (MUC1-A) and 10 μL of 3.0 U μL^{-1} Exo III at 37 °C for 2 h. In this process, S1 could be digested by Exo III accompanied with the release of MUC1-A complex, which was further used to initiate next cleavage process, resulting in the generation of numerous S2. Finally, the resultant solution including various concentrations of S2 and residual Exo III was collected by magnetic separation and stored at 4 °C until further use.

2.5. Assembly of ECL aptasensor

Before use, GCE was pretreated in sequence using 0.3 and 0.05 μm alumina powdery and then cleared thoroughly with deionized water. Then, 15 μL of the CS-Au-DPEA NCs was dropped on the GCE electrode and dried at room temperature to form a CS-Au-DPEA NCs layer. After coating 10 μL of AgNPs on the CS-Au-DPEA NCs/GCE, the obtained electrode was further exposed to 5 μL of 2 μM Fc-HP at 4 °C for 6 h. Following that, 10 μL of HT was used to preclude nonspecific binding. Finally, the HT/Fc-HP/Ag/CS-Au-DPEA NCs/GCE was incubated with 10 μL of mixture including various concentrations of S2 and residual Exo III at 37 °C for 1 h. After being washed, we could use the aptasensor for ECL measurement.

2.6. Measurement procedure

After the construction of ECL aptasensor, the electrode was immersed into 2 mL of PBS (0.1 M, pH 8.0). After that, the working potential from 0 to 1 V (photomultiplier tube (PMT) high-voltage 800 V) with a scan rate of 300 mV s^{-1} was used to the aptasensor for ECL measurement.

3. Results and discussion

3.1. Characterization of Au-DPEA NCs and Ag NPs

The observation of the as-synthesized Au-DPEA NCs was performed by HRTEM. Fig. 1A demonstrated that Au-DPEA NCs have good monodispersity and homogeneity. The size mainly distributed in the range of 1.4–3.8 nm with a mean diameter of 2.54 nm (Fig. 1D). Furthermore, clear lattice fringes of ca.0.230 nm, which was in accord with the (111) facet of Au (Wang et al., 2008), could be easily observed in a high scale HRTEM image of Au-DPEA NCs (Fig. 1B, C). The morphology of the Ag NPs was confirmed by means of SEM and displayed in Fig. S1, which indicated that the Ag NPs exhibited an irregular round shape with size of 100–150 nm.

3.2. Optical Properties of as-synthesized Au-DPEA NCs

The results of photoluminescence (PL) spectra and ECL spectra about as-synthesized Au-DPEA NCs were depicted in Fig. 2. As shown in Fig. 2A, before crosslinking with co-reactant DPEA, the maximum PL emission wavelength of Au NCs (blue line) was at 650 nm. After crosslinking with co-reactant DPEA, the maximum PL emission wavelength of Au-DPEA NCs (red line) slightly red-shifted to 658 nm. Fig. 2B showed the ECL emission spectrum of Au-DPEA NCs (black line) with the maximum emission wavelength at 667 nm. There was about 9 nm red-shift as compared to the PL emission spectra of Au-DPEA NCs, which might be the effect of instrument. In addition, insert in Fig. 2B showed the images of Au-DPEA NCs under visible-light irradiation and UV-light irradiation (λex = 365 nm). It can be seen that the Au-DPEA NCs dispersion was pale brown under white light and turn to rose red under UV lamp.

3.3. ECL performance of Au-DPEA NCs

To confirm the superiority of the self-enhanced Au-DPEA NCs, the ECL performances of (a) Au NCs with direct addition of 5 mM DPEA

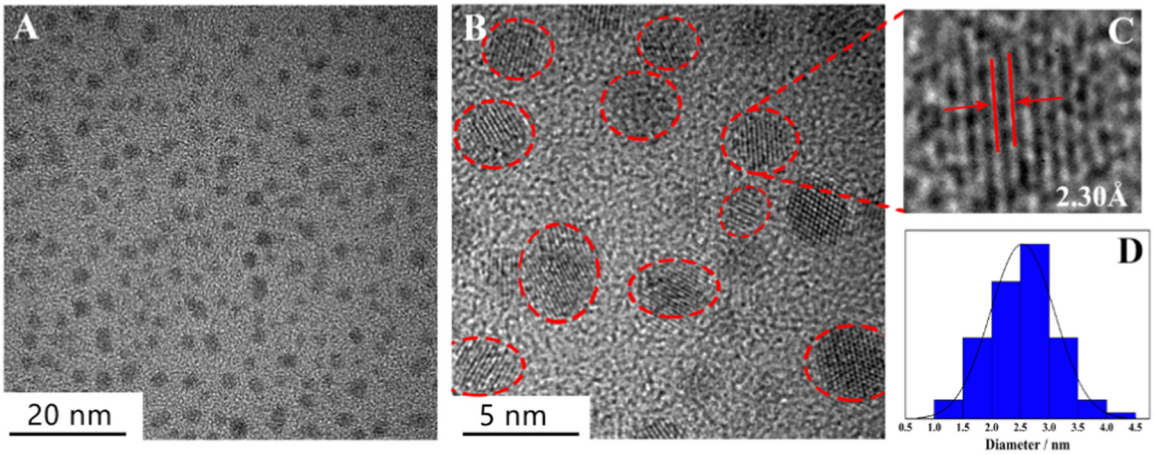

Fig. 1. TEM of Au-DPEA NCs with 20 nm scale (A), HRTEM of Au-DPEA NCs with 5 nm scale (B). The crystalline structure (C) and size distribution of Au-DPEA NCs (D).

(intermolecular reaction pattern), (b) Au-DEDA NCs (self-enhanced pattern with DEDA as co-reactant) and (c) Au-DPEA NCs (self-enhanced pattern with DPEA as co-reactant) were explored. As shown in Fig. 3A, an ECL intensity of 955 a.u. was obtained from Au NCs in PBS containing 5 mM DPEA (curve a). Furthermore, the ECL intensity of self-enhanced Au-DEDA NCs was 1345 a.u. (curve b). Notably, self-enhanced Au-DPEA NCs showed 2048 a.u. of ECL intensity in PBS (curve c), which obviously increased by about 2.1 times and 1.5 times compared to intermolecular reaction pattern and self-enhanced Au-DEDA NCs, respectively, indicating that the self-enhanced structure possessed better ECL performance and the proposed co-reactant DPEA could drastically enhance the ECL intensity of Au NCs compared to DEDA. Finally, CV was used to further characterize the electrochemical properties of DPEA and DEDA. As shown in Fig. 3B, the oxidation peak of DPEA (0.937V, curve a) was lower than that of DEDA (1.067V, curve b), which indicated that the DPEA could be more easily oxidized to $DPEA^{\bullet+}$ to obtain more reductive intermediate radical.

3.4. Possible ECL emitting mechanism of Au-DPEA NCs

For studying the ECL mechanism of the Au-DPEA NCs, the corresponding ECL and CV behavior of Au NCs, Au-DPEA NCs in PBS (0.1 M, pH 8.0) were measured. As shown in 4A, almost no ECL signal was observed from the Au NCs. As DPEA covalently linked with Au NCs, an ECL intensity of 2048 a.u. was obtained through electrode oxidation (Fig. 4B). Meanwhile, an irreversible oxidation peak appeared at 0.92 V from the CV of Au-DPEA NCs. In this process, Au-DPEA NCs was first oxidized by electrode to form the Au^{+}-$DPEA^{\bullet+}$ NCs. Immediately, the Au^{+}-$DPEA^{\bullet+}$ NCs became the intermediate Au^{+}-$DPEA^{\bullet}$ NCs after deprotonation, which could further change to the excited state Au*-DPEA NCs through the intramolecular electron transfer and energy transmission. Finally, the excited state Au*-DPEA NCs returned to ground state Au-DPEA NCs with strong ECL emission. The possible ECL mechanism may be as eqs. 1–4:

$$\text{Au-DPEA NCs} \rightarrow \text{Au}^{+}\text{-DPEA}^{\bullet+}\ \text{NCs} \quad (1)$$

$$\text{Au}^{+}\text{-DPEA}^{\bullet+}\ \text{NCs} \rightarrow \text{Au}^{+}\text{-DPEA}^{\bullet}\ \text{NCs} \quad (2)$$

$$\text{Au*-DPEA NCs} \rightarrow \text{Au-DPEA NCs} + h\nu \quad (4)$$

3.5. Performance of the proposed aptasensor

Under the optimal reaction conditions, the linear range of the designed method for MUC1 was examined. As exhibited in Fig. 5A, the ECL intensities were increased with increasing MUC1 concentration. Furthermore, as shown in Fig. 5B, ECL intensity correlates linearly to the logarithm of MUC1 concentration in the range from 1 fg mL^{-1} to 1 ng mL^{-1} with a correlation coefficient of 0.9981. The regression equation was $\Delta I = 5061.2 + 596.3\ \lg c_{MUC1}$ with a limit detection of 0.54 fg mL^{-1}. Table 1 showed previous studies for MUC1 detection, in which our work exhibited better sensitivity compared to that of others.

The stability of the sensing system was evaluated under continuous 10 cyclic scans at 1 fg mL^{-1} and 100 fg mL^{-1} MUC1, respectively. As exhibited in Fig. 5C, the aptasensor displayed steady signals with relative standard deviations (RSD) of 1.1% and 2.4%, respectively. Moreover, the intra-assay and inter-assay of the sensing system were examined with 100 fg mL^{-1} MUC1. The RSD were 2.1% and 3.5% ($n = 5$), respectively, showing acceptable fabrication reproducibility of the aptasensor (Supplementary Material, Fig. S8).

The selectivity was further evaluated by comparing the ECL response in the presence of different proteins and the results were shown in Fig. 5D. The CEA and AFP caused negligible ECL response. However, we can see that the target MUC1 exhibited a much stronger ECL signal than other interferences samples. Furthermore, the ECL intensity of the mixture had no remarkable difference compared to MUC1. This demonstrated that the proposed aptasensor was selective for MUC1 detection.

3.6. Serum sample measurement

The recovery experiment was performed to assess the applicability of the aptasensor for the analysis of real samples. Firstly, the diluted solution of serum (VSerum/VPBS solution) = 1:50) was used to prepare various concentrations of MUC1. Then, the aptasensor was incubated

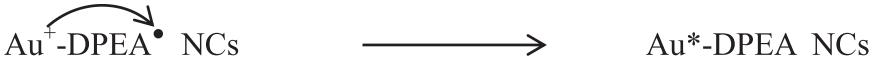

(3)

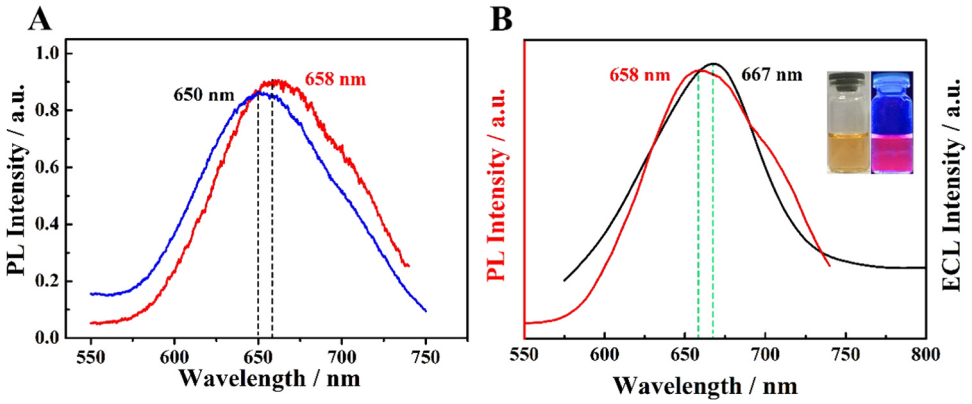

Fig. 2. (A) The maximum PL emission of Au NCs (blue line) and Au-DPEA NCs (red line). (B) ECL emission spectrum of Au-DPEA NCs (black line) and PL emission of Au-DPEA NCs (red line). Inset in B was the image of Au-DPEA NCs under white light and UV light irradiation (λex = 365 nm).

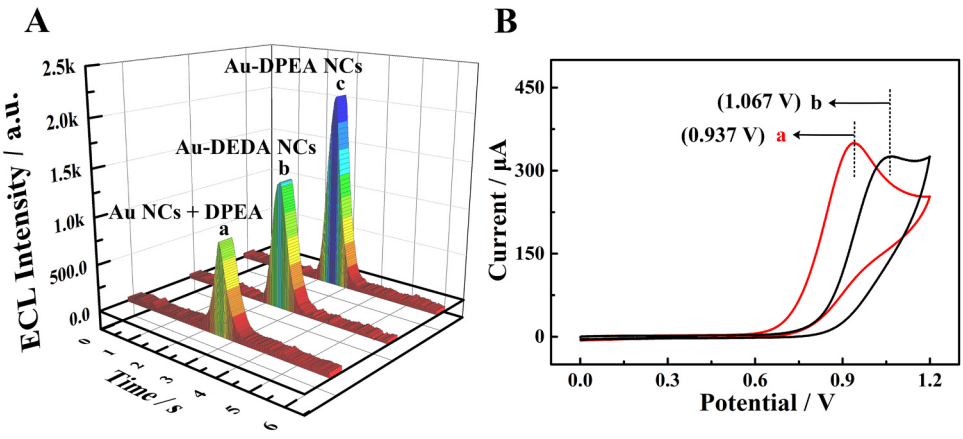

Fig. 3. (A) ECL response of (a) 30 μg mL^{-1} Au NCs with direct addition of 5 mM DPEA, (b) Au-DEDA NCs (30 μg mL^{-1} Au NCs with 5 mM DEDA covalently attached) and (c) Au-DPEA NCs (30 μg mL^{-1} Au NCs with 5 mM DPEA covalently attached) in 2 mL PBS (pH 8.0). (B) cyclic voltammograms of 5 mM DPEA (a) and 5 mM DEDA (b) in 2 mL PBS (pH 8.0).

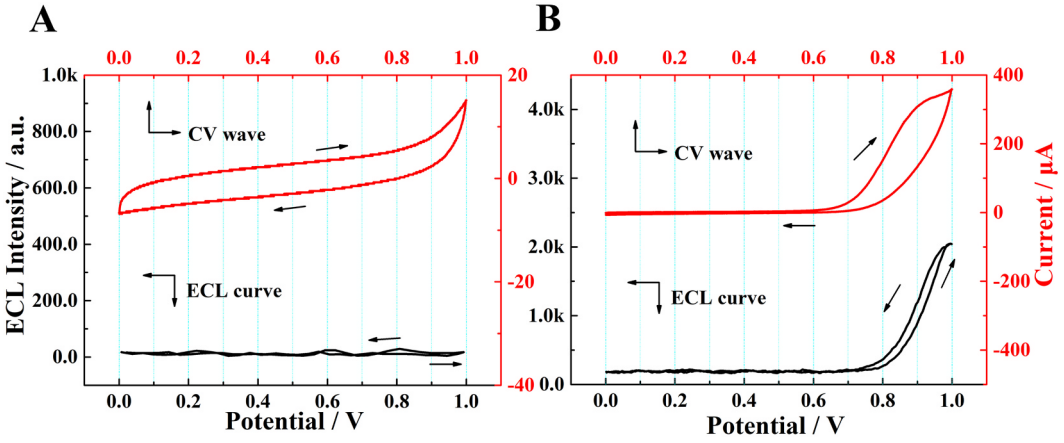

Fig. 4. ECL-potential and corresponding CV curves of Au NCs (A) and Au-DPEA NCs (B) in 0.1 M PBS (pH 8.0).

with the above samples to investigate the influence of the serum samples for MUC1 detection and the results were listed in Table S1 in the Supplementary Material. The recoveries were ranged from 103.8% to 114.6% for serum samples, suggesting that the developed aptasensor was suitable for the determination of MUC1 in clinical application.

4. Conclusion

In summary, the as-synthesized self-enhanced Au-DPEA NCs with high ECL efficiency were successfully applied to establish an ECL aptasensor for the ultrasensitive detection of MUC1. The self-enhanced structure could achieve significant improvement in ECL efficiency by eliminating the use of additional excess co-reactants, shortening the electronic transmission distance, and effectively reducing the loss of energy. In addition, an efficient Exo III propelled multi-site landing DNA walker could convert a small number of target protein to plenty of intermediate DNA to achieve sensitive detection of different targets. In view of these advantages, the self-enhanced metal NCs with high-performance could open a new avenue for the development of metal NCs-based ultrasensitive ECL platform for the biomolecules detection in clinical analysis.

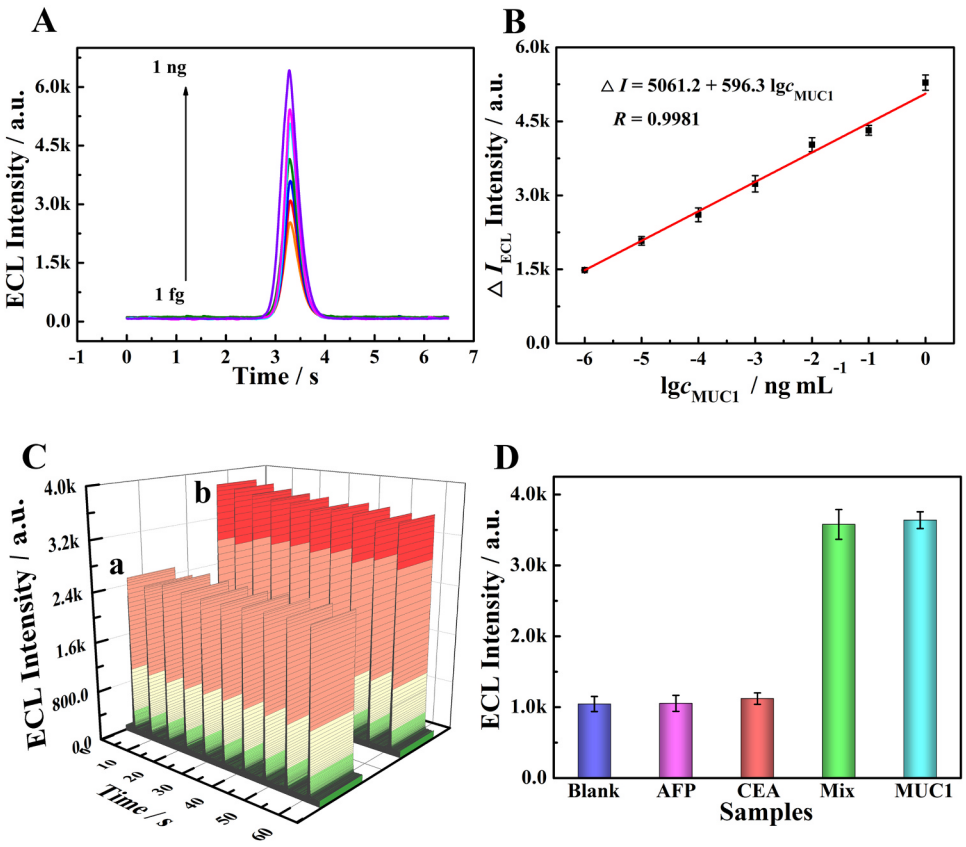

Fig. 5. (A) ECL responses of the sensing system for the target MUC1 at varying concentrations. (B) Linear relationship between the ECL response and the logarithm of MUC1 concentration. (C) Stability of the aptasensor toward 1 fg mL^{-1} (a) and 100 fg mL^{-1} (b) MUC1 under continuous scanning. (D) Selectivity of the proposed aptasensor toward different interferences (1 pg mL^{-1} AFP, 1 pg mL^{-1} LN, 100 fg mL^{-1} MUC1, mixture containing 1 pg mL^{-1}AFP, 1 pg mL^{-1} LN, and 100 fg mL^{-1} MUC1).

Table 1
Comparison of the proposed strategy with other protein detection methods.

Method	Linear range	Target	Detection limit	Ref
EC	10^{-3}–100 μM	MUC1	2.48 μg mL^{-1} (0.827 nM)	Deng et al. (2017)
FL	10^{-1}–12 ng mL^{-1}	MUC1	0.0748 ng mL^{-1}	Si et al. (2018)
SRES	10–10^{8} fg mL^{-1}	MUC1	10 fg mL^{-1}	Kamil Reza et al. (2017)
PEC	10^{-2}–40 ng mL^{-1}	CEA	3.6 pg mL^{-1}	Qiu et al. (2018)
ECL	0.05–20 ng mL^{-1}	AFP	6.2 pg mL^{-1}	Wang et al. (2018)
ECL	10–10^{7} fg mL^{-1}	MUC1	2.8 fg mL^{-1}	Jiang et al. (2016)
ECL	10^{-1}–10^{6} fg mL^{-1}	MUC1	0.54 fg mL^{-1}	This work

Acknowledgement

This work was financially supported by the National Natural Science Foundation of China (21775124, 21675129 and 21575116), Chongqing Graduate Scientific Research Innovation Project (CYB17061). The Fundamental Research Funds for the Central Universities (XDJK2018AA003, XDJK2018C041) and the Chongqing Research Program of Basic Research and Frontier Technology (cstc2017jcyjAX0230), China.

Credit author statement

Fang Yang and Xia Zhong conceived and designed the experiments. Fang Yang performed most of the experiments, contributed to experimental design, data analysis and wrote the manuscript. Ying Zhuo and Xinya Jiang reviewed the original draft. Shaping Wei and Ruo Yuan supervised the study. All authors discussed the results and commented on the manuscript.

Declaration of interests

None.

Appendix A. Supporting information

Supplementary data associated with this article can be found in the online version at https://doi.org/10.1016/j.bios.2019.01.057.

References

Aldeek, F., Muhammed, M.H., Palui, G., Zhan, N., Mattoussi, H., 2013. ACS Nano 7, 2509–2521.
Bath, J., Green, S.J., Turberfield, A.J., 2005a. Angew. Chem. Int. Ed. 44, 4358–4361.
Bath, J., Green, S.J., Turberfield, A.J., 2005b. Angew. Chem. Int. Ed. 117, 4432–4435.
Cha, T.G., Pan, J., Chen, H.R., Salgado, J., Li, X., Mao, C.D., Choi, J.H., 2014. Nat. Nanotechnol. 9, 39–43.
Chen, A.Y., Gui, G.F., Zhuo, Y., Chai, Y.Q., Yuan, R., 2015. Anal. Chem. 87, 6328–6334.
Chen, D., Luo, Z., Li, N., Lee, J.Y., Xie, J., Lu, J., 2013. Adv. Funct. Mater. 23, 4324–4331.
Deng, C.Y., Pi, X.M., Qian, P., Chen, X.Q., Wu, W.M., Xiang, J., 2017. Anal. Chem. 89, 966–973.
Fang, Y.M., Song, J., Li, J., Wang, Y.W., Yang, H.H., Sun, J.J., Chen, G.N., 2011. Chem. Commun. 47, 2369–2371.
Fu, X.M., Tang, X.R., Yuan, R., Chen, S.H., 2017. Biosens. Bioelectron. 90, 61–68.
Jiang, X.Y., Wang, H.J., Wang, H.J., Yuan, R., Chai, Y.Q., 2016. Anal. Chem. 88, 9243–9250.
Jung, C., Allen, P.B., Ellington, A.D., 2016. Nat. Nanotechnol. 11, 157.
Kamil Reza, K., Wang, J., Vaidyanathan, R., Dey, S., Wang, Y., Trau, M., 2017. Small 13, 1602902.
Li, L.L., Liu, H.Y., Shen, Y.Y., Zhang, J.R., Zhu, J.J., 2011. Anal. Chem. 83, 661–665.
Li, P., Jin, Z., Zhao, M., Xu, Y., Guo, Y., Xiao, D., 2015. Dalton Trans. 44, 2208–2216.

Li, S., Ulrich Nienhaus, G., 2012. Bio. Rev. 4, 313–322.
Liang, W.B., Zhuo, Y., Xiong, C.Y., Zheng, Y.N., Chai, Y.Q., Yuan, R., 2015. Anal. Chem. 87, 12363–12371.
Lin, S.Y., Chen, N.T., Sun, S.P., Chang, J.C., Wang, Y.C., Yang, C.S., Lo, L.W., 2010. J. Am. Chem. Soc. 132, 8309–8315.
Qiu, Z.L., Su, J., Tang, D.P., 2018. Anal. Chem. 90, 1021–1028.
Schmid, G., Bäumle, M., Geerkens, M., Heim, I., Osemann, C., Sawitowski, T., 1999. Chem. Soc. Rev. 28, 179–185.
Si, H.B., Wang, L.J., Li, Q.L., Li, X.X., Li, L., Tang, B., 2018. Chem. Commun. 54, 8277–8280.
Song, W., Wang, Y., Liang, R.P., Zhang, L., Qiu, J.D., 2015. Biosens. Bioelectron. 64, 234–240.
Swanick, K.N., Ladouceur, S., Zysman-Colman, E., Ding, Z., 2012. Angew. Chem. Int. Ed. 51, 11079–11082.
Wang, C., Hu, Y., Lieber, C., Sun, S., 2008. J. Am. Chem. Soc. 130, 8902.
Wang, H.J., Yuan, Y.L., Chai, Y.Q., Yuan, R., 2015a. Biosens. Bioelectron. 68, 72–77.
Wang, L., Deng, R., Li, J., 2015b. Chem. Sci. 6, 6777–6782.
Wang, T., Wang, D., Padelford, J.W., Jiang, J., Wang, G., 2016. J. Am. Chem. Soc. 138, 6380–6383.
Wang, X.F., Gao, H.F., Qi, H.L., Gao, Q., Zhang, C.X., 2018. Anal. Chem. 90, 3013–3018.
Wickham, S.F.J., Bath, J., Katsuda, Y., Endo, M., Hidaka, K., Sugiyama, H., Turberfield, A.J., 2012. Nat. Nanotechnol. 7, 169–173.
Yang, J.M., Dou, B.T., Yuan, R., Xiang, Y., 2017. Anal. Chem. 89, 5138–5143.
Yehl, K., Mugler, A., Vivek, S., Liu, Y., Zhang, Y., Fan, M.Z., Weeks, E.R., Salaita, K., 2016. Nat. Nanotechnol. 11, 184–190.
Yue, L., Wang, S., Cecconello, A., Lehn, J.M., Willner, I., 2017. ACS Nano 11, 12027–12036.
Zhang, P., Jiang, J., Yuan, R., Zhuo, Y., Chai, Y.Q., 2018. J. Am. Chem. Soc. 140, 9361–9364.
Zhou, C., Duan, X.Y., Liu, N., 2015. Nat. Commun. 6, 8102.